View Online / Journal Homepage / Table of Contents for this issue
Dynamic Article Links

Journal of
Materials Chemistry

Cite this: *J. Mater. Chem.*, 2012, **22**, 15606

www.rsc.org/materials

PAPER

Magnetic properties of Fe_2GeMo_3N; an experimental and computational study

Peter D. Battle,[*a] **Lev A. Sviridov,**[a] **Russell J. Woolley,**[a] **Fernande Grandjean,**[b] **Gary J. Long,**[c] **C. Richard A. Catlow,**[d] **Alexey A. Sokol,**[d] **Aron Walsh**[d] **and Scott M. Woodley**[d]

Received 24th April 2012, Accepted 21st June 2012
DOI: 10.1039/c2jm32574h

A polycrystalline sample of Fe_2GeMo_3N has been synthesized by the reductive nitridation of a mixture of binary oxides in a flow of 10% dihydrogen in dinitrogen. The reaction product has been studied by magnetometry, neutron diffraction and Mössbauer spectroscopy over the temperature range $1.8 \leq T/\mathrm{K} \leq 700$. The electronic structure and magnetic coupling have been modelled by Density Functional Theory (DFT) and Monte Carlo methods. Fe_2GeMo_3N adopts the cubic η-carbide structure with $a = 11.1630(1)$ Å at 300 K. The electrical resistivity was found to be ~0.9 mΩ cm over the temperature range $80 \leq T/\mathrm{K} \leq 300$. On cooling below 455 K the compound undergoes a transition from a paramagnetic to an antiferromagnetic state. The magnetic unit cell contains an antiferromagnetic arrangement of eight ferromagnetic Fe_4 tetrahedra; the ordered atomic magnetic moments, 1.90(4) μ_B per Fe atom at 1.8 K, align along a <111> direction. DFT predicts an ordered moment of 1.831 μ_B per Fe. A random phase approximation to the DFT parameterised Heisenberg model yields a Néel temperature of 549 K, whereas the value of 431 K is obtained in the classical limit for spin. Monte Carlo calculations confirm that the experimentally determined magnetic structure is the lowest-energy antiferromagnetic structure, but with a lower Néel temperature of 412 K. These results emphasise the potential of these computational methods in the search for new magnetic materials.

1. Introduction

Nitrides with the so-called η-carbide structure,[1] for example Fe_3Mo_3N and Co_3Mo_3N, have been the subject of many recent studies that have addressed either their mechanical properties and hardness,[2,3] their catalytic activity[4–8] or their electrical[9] and magnetic properties.[10–13] Our interest lies in the latter. Although an earlier study[14] reported that Fe_3Mo_3N is antiferromagnetic below 120 K, the most recent neutron diffraction and Mössbauer data[11] show convincingly that no long-range magnetic order is present at 4.5 K. The temperature dependence of the electrical resistivity and the specific heat led Waki *et al.* to describe this compound as behaving like a non-Fermi liquid close to a ferromagnetic quantum critical point. The isostructural compound Co_3Mo_3N has been described as a Pauli paramagnet, with the absence of long-range magnetic order having been proved by nuclear magnetic resonance spectroscopy.[10]

A study[15] of the mixed-metal system $Fe_{3-x}Co_xMo_3N$ revealed a large enhancement of the magnetisation of $Fe_{2.5}Co_{0.5}Mo_3N$ below 30 K in a field of 100 Oe, but no evidence for long-range magnetic order was apparent in neutron diffraction data collected at 5 K; the compound was described as a superparamagnet. It was also observed that the distribution of iron and cobalt over the two available sites in the structure was not random. The sites in question are the 16*d* and 32*e* sites of the cubic space group $Fd\bar{3}m$. The atoms on the 32*e* sites occur in tetrahedral groups with each face of every tetrahedron being capped by an atom on a 16*d* site, thus forming a supertetrahedron; the supertetrahedra share vertices to form an infinite diamondoid net, as shown in Fig. 1. The molybdenum atoms occupy a 48*f* site and form a network of vertex-sharing Mo_6 octahedra, with a nitrogen atom occupying an interstitial 16*c* site at the centre of each octahedron. The complete structure can thus be said to consist of two interpenetrating networks with the stoichiometries M_2M' and Mo_3N, where M and M′ represent the elements on the 32e and 16*d* sites, respectively. In the case of $Fe_{3-x}Co_xMo_3N$, iron showed a significant preference for the 16*d* site although a disordered distribution was always observed, even in $FeCo_2Mo_3N$.

We have previously attempted to modify the chemical composition of these η-carbide phases in various ways in order to access the apparently latent ferromagnetic ground state. One

---

[a] *Inorganic Chemistry Laboratory, Oxford University, South Parks Road, Oxford, OX1 3QR, UK. E-mail: peter.battle@chem.ox.ac.uk*
[b] *Faculty of Sciences, University of Liège, B-4000 Sart – Tilman, Belgium*
[c] *Department of Chemistry, Missouri University of Science and Technology, University of Missouri, Rolla, MO 65409-0010, USA*
[d] *Department of Chemistry, University College London, 20 Gordon Street, London, WC1H 0AY, UK*

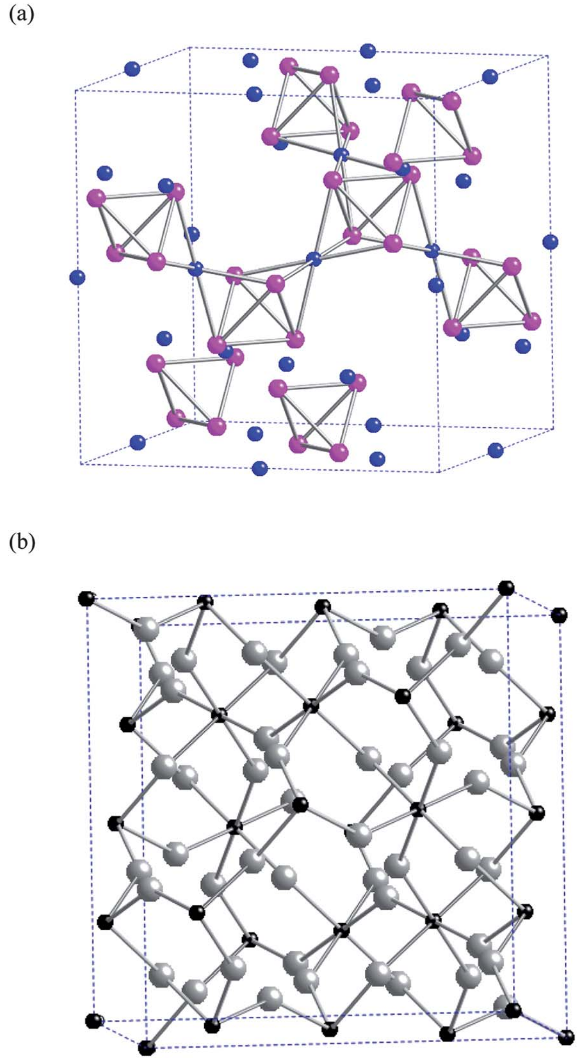

Fig. 1 The networks of (a) 32*e* (magenta) and 16*d* (blue) sites and (b) 48*f* (large grey circles) and 16*c* sites (small black circles) in the η-carbide structure.

strategy involved the introduction of a diamagnetic cation onto the 16*d* site, so that the only exchange interactions were those between atoms on the 32*e* sites. This approach resulted[12] in the adoption of a magnetically ordered ground state by some compositions in the system $Fe_{2-x}Co_xGe_{1-y}Ga_yMo_3N$, but the ordering was antiferromagnetic rather than ferromagnetic. The highest Néel temperatures were observed in the $y = 0$ compounds $Fe_{2-x}Co_xGeMo_3N$, although the value of T_N was very sensitive to the composition. More specifically, Co_2GeMo_3N was found not to show long-range magnetic order, although a magnetic transition to what was assumed to be a spin-glass state was observed at 8 K. In contrast, $Fe_{1.5}Co_{0.5}GeMo_3N$ was shown to be antiferromagnetic at room temperature. The actual Néel temperature was not determined and no samples with higher iron contents were discussed. We have now synthesized Fe_2GeMo_3N and characterized it by magnetometry and neutron diffraction. The resulting data have been used to assess the relative applicability of Density Functional Theory (DFT) and Monte Carlo (MC) calculations to this system.

2. Experimental

Polycrystalline samples of Fe_2GeMo_3N were synthesized by firing intimately ground, stoichiometric mixtures of iron(III) oxide, molybdenum(VI) oxide and germanium(IV) oxide in an alumina crucible under a flow of 10% dihydrogen in dinitrogen. The mixture was initially fired as a loose powder at 973 K and then pressed into pellets for subsequent firings at temperatures of up to 1248 K. The reaction product was always cooled to room temperature under the gas flow. The progress of the reaction was monitored by X-ray powder diffraction. Data suitable for unit-cell parameter determination by Rietveld analysis[16] were collected from the final product on a Philips X'Pert PRO diffractometer using Cu Kα_1 radiation. The angular range $5 \le 2\theta/° \le 125$ was scanned with a step size $\Delta 2\theta = 0.0084°$. The data were analysed using the GSAS program suite.[17]

The magnetic properties of the product were studied using a Quantum Design MPMS 5000 SQUID magnetometer. The sample magnetisation was measured in a field of 1000 Oe over the temperature range $300 \le T/\mathrm{K} \le 700$ and in a field of 100 Oe over the temperature range $2 \le T/\mathrm{K} \le 350$. In both cases the sample was initially held at the high-temperature limit (700 or 350 K) and then cooled in the absence of an applied field to the low-temperature limit (300 or 2 K). Data were then collected during warming. The sample was then re-cooled in the measuring field and a second data set was collected on re-warming.

Electrical resistivity measurements were carried out over the temperature range $80 \le T/\mathrm{K} \le 300$ using a four-probe d.c. technique; data were collected on warming. The sample was in the form of a rectangular block, approximately 10 × 4 × 2 mm in size, which had been cut from a sintered pellet of the reaction product. Copper wires were attached to the block using a silver-loaded epoxy adhesive resin. The measurement was carried out using a constant current, selected to lie in the range $10 \le I/\mathrm{mA} \le 90$. Duplicate measurements on blocks cut from different pellets showed the same qualitative temperature dependence but the magnitude of the resistivity varied by approximately 25%. Our ability to offer a quantitative interpretation of the resistivity data given below is limited by this variability, which presumably stems from grain-boundary effects in the sintered blocks.

Neutron diffraction data were recorded from a selected sample at thirty-two temperatures in the range $1.8 \le T/\mathrm{K} \le 300$ using the powder diffractometer D20 at ILL, Grenoble. Data were collected using a wavelength of ~1.36 Å if the principal purpose of the measurement was to study the crystal structure, or ~1.86 Å if the principal purpose was to search for magnetic scattering at relatively high *d*-spacings; the unit-cell parameter determined from X-ray powder diffraction data was used to determine a more accurate value for the neutron wavelength in each case. The sample, of mass ~1.5 g, was contained in a vanadium can of diameter 5 mm. The data were analysed using the GSAS program suite. The peak shape was modelled using a pseudo-Voigt function and the background level by a twelve-term Chebyshev polynomial.

The Mössbauer spectra of Fe_2GeMo_3N have been measured at 10 and 295 K in a Janis Supervaritemp cryostat with a constant-acceleration spectrometer which utilized a rhodium matrix cobalt-57 source and was calibrated at 295 K with α-iron powder. The Mössbauer spectral absorbers contained 40 mg cm^{-2} of finely ground powder mixed with boron nitride. The statistical errors associated with the isomer shifts, quadrupole splittings, hyperfine fields, and line widths are tabulated below; the absolute errors of these parameters are approximately twice the statistical errors.

3. Computational methods

DFT calculations were performed for Fe_2GeMo_3N using the VASP[18,19] code, with periodic boundary conditions used to represent the infinite solid. For the description of electron exchange and correlation, the PBEsol functional[20] was used within the generalised gradient approximation. The PBEsol functional has been shown, for a range of materials, to result in lattice parameters in much better agreement with experiment than other local or semi-local exchange-correlation functionals. The applicability of the alternative hybrid density functionals to metallic or semi-metallic materials remains a contentious issue due to the failure of the underlying Hartree–Fock method in the description of partially occupied bands. A plane-wave basis set with an upper energy threshold of 500 eV was selected as it offered convergence in both the total energy and structural parameters. Various k-point grids were tested for the Brillouin zone integration; a 6 × 6 × 6 grid was found to be sufficient. The valence–core interactions were modelled using the projector augmented-wave (PAW) method,[21] with the appropriate core being selected for each element; Fe, Ge–[Ar]; Mo–[Kr]; N–[He]. The 3d states of Ge were treated explicitly as valence electrons. For each calculation, the ground-state total energies and equilibrium structures were obtained by full relaxation of the atomic positions and the volume of the unit cell to minimise the quantum mechanical stresses and forces (forces < 0.01 eV/Å). The lattice parameter and interatomic distances were then compared to experimental values derived from neutron diffraction data collected at 3.5 K. To calculate the charge on each atom, Bader charge density analysis[22,23] was carried out. This procedure attributes charge to atomic centres based on the definition of atomic basins: regions in the material enclosing individual atoms and whose boundary is defined by zero density gradient. The density of electronic states was also calculated.

Both antiferromagnetic (AFM) and ferromagnetic (FM) ordering of the atomic magnetic moments located on the 32e sites were considered. As is detailed below, the total energy of each configuration was calculated, with the lower in energy being the preferred magnetic structure and the magnitude of the energy difference, $E_{AFM} - E_{FM}$, giving an indication of the strength of the magnetic coupling and, in turn, the temperature of the magnetic transition. For FM ordering all spins were set to be parallel; the number of unpaired electrons per site, and hence the magnetic moment of the system, was optimised self-consistently. In the case of AFM ordering, several starting models, all with collinear spin systems, were tried. For each model the spins were relaxed with the constraint that the sum of the atomic magnetic moments over the unit cell was zero. The different models all converged to the antiferromagnetic arrangement of ferromagnetically aligned $(32e)_4$ tetrahedra that was observed experimentally in the case of $Fe_{1.5}Co_{0.5}GeMo_3N$ (ref. 12).

To estimate the temperature of the phase transition we used the standard Heisenberg Hamiltonian in atomic units

$$H = -J\sum{}' \hat{S}_i\hat{S}_j,$$

with $J > 0$ describing ferromagnetic and $J < 0$ antiferromagnetic interactions, and where the lattice sum includes all spin pairs (i ≠ j); $2JS_iS_j$ gives the exchange interaction energy between spins i and j. We also assumed that the interactions are only between nearest neighbours, and are symmetry equivalent, even if there are small differences in magnetic moments or geometric parameters. For ferromagnetic systems, we used the ground state energy E_{FM} and the energy of a broken symmetry solution, or Neel state, for antiferromagnetic:

$$E_{FM} = -JzS^2N,$$

and

$$E_{AFM} = +JzS^2N,$$

where z is the coordination number and N is the number of spins in our system. Then

$$Jz = \frac{E_{AFM} - E_{FM}}{2NS^2}$$

When mapping our calculation onto the Heisenberg Hamiltonian, we used a unit cell with eight tetrahedra comprising 32e sites, each tetrahedron bearing spin $S = \frac{1}{2}n*4 = 2n$, where n, determined by the DFT calculations, is the number of unpaired electrons per atom; each tetrahedron has $z = 4$ nearest-neighbour tetrahedra. We thus treated each tetrahedron as a ferromagnetic unit and assigned to it a single, total spin value. Our approach, therefore, results in a single exchange constant, J, that measures the coupling between the total spins of neighbouring tetrahedra.

The critical temperature within the mean-field approximation, MFA, (Van Vleck's formula) is:

$$T_c = \frac{2}{3}\frac{Jz}{k_B}S(S+1) = \frac{E_{AFM} - E_{FM}}{3k_BN}\frac{S+1}{S}$$

Due to the symmetry between the ferromagnetic and antiferromagnetic Neel states, expressions for the critical temperatures are identical at this level of approximation. More advanced calculations using a higher level of theory within the random-phase approximation, RPA, result in a reduced critical temperature. The reduction factor depends on the structure and typically lies between $^2/_3$ and $^3/_4$.

In view of the questionable reliability of RPA methods when applied to AFM systems, we carried out classical Monte Carlo simulations for the systems of interest with the code Spinner 1.0 (ref. 24) using the parameterised Heisenberg Hamiltonian. Two models were investigated. In model 1, the transition-metal tetrahedra were represented by single classical spins, as they were in the analytical treatment described above. In model 2, the atoms within the tetrahedra were considered explicitly. This approach necessitated the introduction of coupling constants J_i both for nearest neighbours (nn) within the same tetrahedron and next-nearest neighbours (nnn) in neighbouring tetrahedra. The interaction, J_1, between iron atoms in the same tetrahedron is a direct exchange whereas that between atoms in two neighbouring Fe_4 tetrahedra, can be thought of as a superexchange interaction involving a bridging Ge atom. There are three Fe–Ge–Fe′ linkages between each iron atom and each of three neighbouring tetrahedra, two of these linkages have an angle of ~115° at Ge (J_2) and one pathway is linear (J_3), see Fig. 1(a). Thus three coupling constants are required in this model whereas only one, corresponding to $2J_2 + J_3$, was derived from the DFT calculations. Experiment shows that the magnetic coupling in $Fe_{1.5}Co_{0.5}GeMo_3N$ and, as we shall describe below, Fe_2GeMo_3N is FM within the tetrahedra and AFM between adjacent tetrahedra. The ratio $J_1 : J_2 : J_3$ was therefore set to be $-1 : -0.01 : 0.1$ for Fe_2GeMo_3N. The ratio $J_1 : (2J_2 + J_3)$ then reflects the observed low-temperature magnetic properties of this compound; we have assumed that the 180° superexchange parameterised by J_3 is stronger than that represented by J_2. In our MC simulations, the values of J (model 1), $2J_2 + J_3$ (model 2) and the structural parameters were set to those obtained from our DFT calculations. For each system and model, the process of annealing was simulated six times using MC simulations at ~250 temperatures, where at each temperature the system was thermalised before data collection over an additional 50 000 MC steps (sweeps). Note that 9 × 9 × 9 and 6 × 6 × 6 supercells (based on the conventional cubic cell) were used in model 1 and 2, respectively. Thus, we modelled 5832 independent spins for model 1 and 6912 for model 2.

4. Results

(i) Experimental results

The synthesis was repeated a number of times. In each case, the X-ray diffraction pattern of the principal phase in the reaction product could be indexed in space group $Fd\bar{3}m$ and was consistent with the formation of an η-carbide phase of composition Fe_2GeMo_3N. However, a small quantity of an unidentified impurity phase (~1%) was always present. The unit cell parameter of the η-carbide phase refined to a value of $a_0 = 11.1630(1)$ Å. Elemental analysis showed the nitrogen content of the products to lie between 2.8 and 3.0 ± 0.1%, in good agreement with the value of 2.88% calculated for Fe_2GeMo_3N.

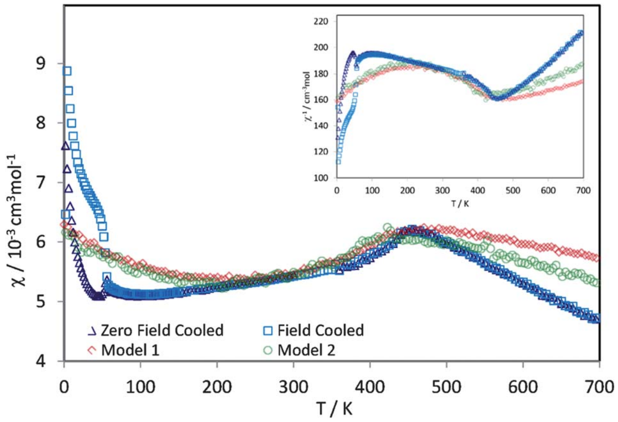

Fig. 2 Experimental and calculated temperature dependence of the molar magnetic susceptibility of Fe_2GeMo_3N; the inverse susceptibility is shown in the inset.

The temperature dependence of the molar magnetic susceptibility of a typical sample of Fe_2GeMo_3N is shown in Fig. 2. The susceptibility passes through a maximum at 455 K and a second transition occurs at 56 K. Hysteresis between the zero-field-cooled and field-cooled data is apparent below the latter, but no such effect is seen close to the former. All samples showed some hysteresis at low temperatures, but the extent of the effect varied from sample to sample. The electrical resistivity of this composition was found to be ~0.9 mΩ cm throughout the measured temperature range.

The neutron diffraction pattern collected over the angular range $15 < 2\theta/° < 140$ at 300 K using a wavelength of 1.36 Å was also consistent with the presence of an η-carbide phase. Rietveld analysis showed that the 16*d* and 32*e* sites were exclusively occupied by germanium and iron, respectively. Test refinements showed that the concentration of vacancies on the nitrogen 16*c* site is too small to be measured (<1.5%), as is the concentration of nitrogen atoms on the alternative 8*a* site.[8] The refined structural parameters are listed in Table 1 and the observed and calculated diffraction profiles are shown in Fig. 3(a). The unfitted peak at $2\theta \sim 52°$ is likely to derive from the minority phase that was detected by X-ray diffraction. The agreement factors R_{wp} and R_I took values of 3.9% and 4.2%, respectively when 125 reflections were used in the structure analysis. Bragg scattering that could not be accounted for by this structural model was apparent at low angles, most notably in the forbidden 200 reflection, in neutron diffraction data collected at the same temperature using a wavelength of 1.86 Å, see Fig. 3(b). In the light of the susceptibility data described above, this scattering was assumed to be magnetic in origin. It could be accounted for by a magnetic structure consisting of an F-centred antiferromagnetic arrangement of ferromagnetic Fe_4 tetrahedra, as shown in Fig. 4. No abrupt change in the diffraction pattern was observed when the sample was cooled below 56 K, and the same magnetic model could account for data collected at all temperatures. The ordered magnetic moment refined to values of 1.52(4) and 1.90(4) μ_B per iron atom at 300 and 1.8 K, respectively. The unit cell parameter at 1.8 K, refined from data collected using a wavelength of ~1.86 Å, was found to be 11.1475(1) Å.

The iron-57 Mössbauer spectra of three different reaction products were measured at 295 K and found to be superimposable. It was therefore concluded that the variable concentration of any impurity phase in Fe_2GeMo_3N had no significant effect on the spectra, and one sample was selected for more detailed study at 10 K. The resulting spectra are shown in Fig. 5.

The spectra indicate that Fe_2GeMo_3N exhibits long-range magnetic order at both 10 and 295 K and that the crystallographically equivalent 32*e* iron sites are not magnetically

Table 1 Structural parameters of Fe_2GeMo_3N at 300 K determined by neutron diffraction[a]

	site	*x*	*y*	*z*	U_{iso}/Å^2
Fe	32*e*	0.29169(7)	0.29169(7)	0.29169(7)	0.51(2)
Ge	16*d*	1/2	1/2	1/2	0.50(4)
Mo	48*f*	0.3181(1)	1/8	1/8	0.48(3)
N	16*c*	0	0	0	0.58(3)

[a] Space group $Fd\bar{3}m$, $R_{wp} = 2.5\%$, $R_I = 4.2\%$, $\chi^2 = 15.71$.

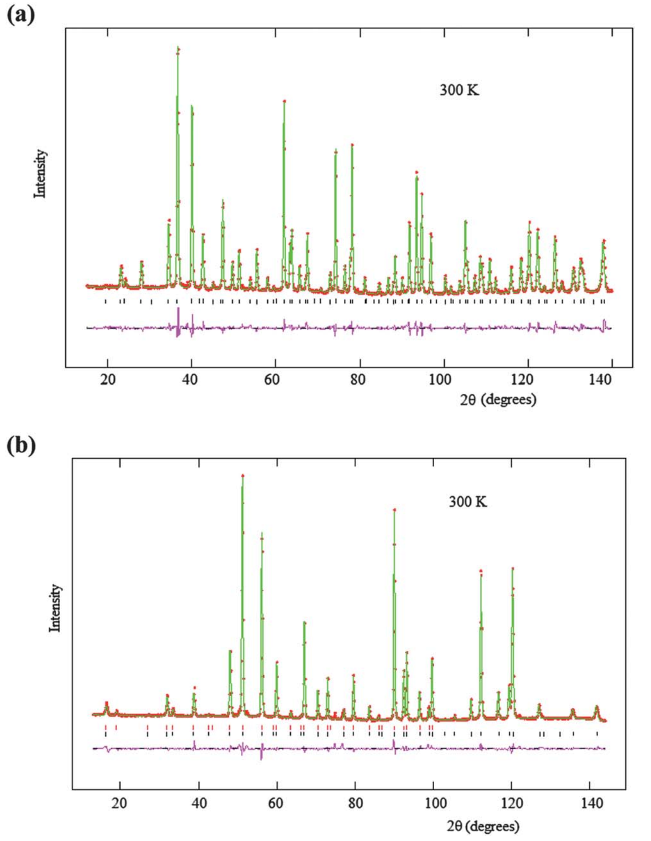

Fig. 3 Observed and calculated neutron diffraction profiles of Fe_2GeMo_3N at 300 K using (a) $\lambda = 1.36$ Å and (b) $\lambda = 1.86$ Å; a difference curve is also shown. Reflection positions are marked in both cases; the upper set of markers in (b) indicates magnetic reflections.

equivalent in the presence of the internal hyperfine field but are divided into two types of magnetic site in an 8 : 24 ratio. We hypothesized that the magnetic inequivalency occurs because the principal axis of the electric field gradient, V_{zz}, makes different angles, θ, with the internal hyperfine field of Fe_2GeMo_3N such that the θ values at 75% of the iron sites are the same and different from those at the remaining 25%. As a consequence of this inequivalency, the Mössbauer spectra of Fe_2GeMo_3N have been fit by using two sextets in a fixed area ratio of 8 : 24 with the same line width, isomer shift, quadrupole interaction, $\Delta E_Q = e^2Qq/2$, and asymmetry parameter, η, and different hyperfine fields and θ angles. Because of the $3m$ point symmetry at the 32e iron site in Fe_2GeMo_3N, it is reasonable to assume that V_{zz} at each iron site is oriented along the local 3-fold axis, an axis that is along one of the <111> axes. Hence, the principal axes at the four sites within each Fe_4 tetrahedron will be 109° degrees apart. Then, if the magnetic moments of the four iron atoms in every tetrahedron and, hence, the internal hyperfine field, are oriented along just one of the <111> axes, say the [111] axis, one iron site in each tetrahedron will have a θ angle of 0° and the remaining three iron sites will have θ angles of 71°. Thus the Mössbauer spectra of Fe_2GeMo_3N have been fitted with two magnetic components with an area ratio of 8 : 24 having the same ΔE_Q value and θ values constrained to 0° and 71°. A subsequent fit in which η was allowed to take small non-zero values indicated that the best fits corresponded to $\eta = 0$ as should be the case if V_{zz} at the 32e site in Fe_2GeMo_3N is oriented along a 3-fold axis. The final fits involved the variation of two internal hyperfine fields, H, one isomer shift, δ, one quadrupole interaction, $\Delta E_Q = e^2Qq/2$, one line width, Γ, one dimensionless incremental line width, $\Delta\Gamma$, and one total spectral absorption area, for a total of seven variables. In these fits the incremental line width, $\Delta\Gamma$, is given by $\Gamma_i = \Gamma + (v_i - \delta)\Delta\Gamma$, where v_i is the velocity of the i-th spectral channel in mm s^{-1}. Although the fits with $\Delta\Gamma$ constrained to zero were adequate, the inclusion of the small $\Delta\Gamma$ value clearly improved the spectral fits with little change in the remaining parameters. The small $\Delta\Gamma$ values observed probably result from small variations in the demagnetizing fields in different size particles in the spectral absorber. The resulting fits, see Fig. 5, are excellent and confirm our hypothesis that the spins in every tetrahedra align along a single <111> axis. The corresponding spectral fitting parameters are given in Table 2.

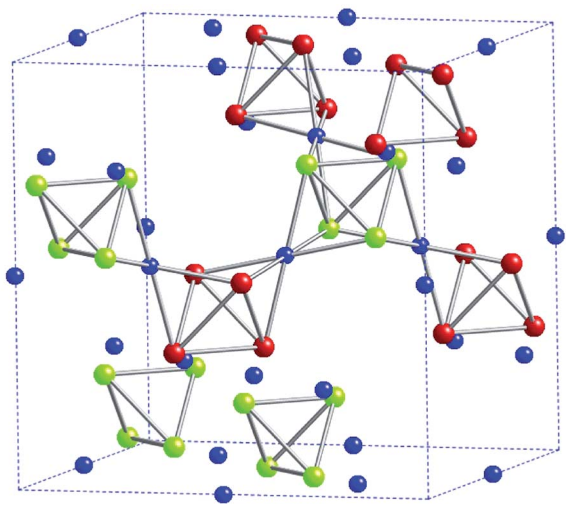

Fig. 4 The antiferromagnetic structure of Fe_2GeMo_3N. Magnetically ordered spin-up and spin-down atoms are shown in red and green; germanium atoms are shown in blue.

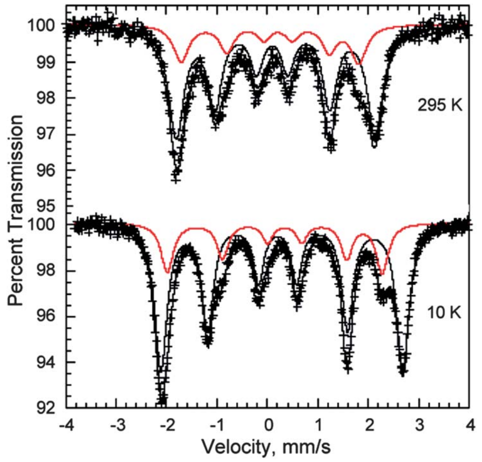

Fig. 5 The Mössbauer spectra of Fe_2GeMo_3N obtained at the indicated temperatures and fit with two components in an area ratio of 1 : 3 with θ-values constrained to 0° and 71° as discussed in the text.

The isomer shifts observed for Fe_2GeMo_3N, in which a given iron has a near-neighbour environment consisting of six

Table 2 Mössbauer spectral parameters for Fe_2GeMo_3N

T, K	H, T	δ, mm s^{-1a}	ΔE_Q, mm s^{-1}	θ, deg	η	Γ, mm s^{-1}	$\Delta\Gamma$	Area%
295^b	12.19(3)	0.130(2)	−0.19(3)	71	0.0	0.30(1)	0.041(8)	75
	10.95(7)	0.130(2)	−0.19(3)	0	0.0	0.30(1)	0.041(8)	25
10^b	14.83(1)	0.243(1)	−0.23(4)	71	0.0	0.246(4)	0.025(2)	75
	13.23(2)	0.243(1)	−0.23(4)	0	0.0	0.246(4)	0.025(2)	25

[a] The isomer shifts are given relative to α-iron powder at 295 K. [b] The fit obtained with θ constrained to the value given and where the quoted errors correspond to the statistical errors.

molybdenum, three germanium, and three iron atoms, are typical of intermetallic compounds and are, as expected, virtually identical to those observed[12] earlier in $Co_{0.5}Fe_{1.5}GeMo_3N$ in which the iron is in a similar near-neighbour environment. At 10 K, the positive isomer shift of 0.244(1) mm s^{-1} relative to α-iron indicates that the s-electron density at the iron nucleus in Fe_2GeMo_3N is smaller than in α-iron. Our density functional calculations show that the electrons responsible for the charge of −0.3 per iron atom on the 32*e* site, see Table 3, occupy 3d orbitals and thus provide an additional screening of the s-electrons and an increased isomer shift. The quadrupole interactions are small, but non-zero, as would be expected from the non-spherical charge distribution obtained from the density functional calculations, see Fig. 6.

Further, the two hyperfine fields of 13.23(2) and 14.83(1) T are typical of intermetallic compounds with the above near-neighbor environment and, again, are very similar to those observed[12] earlier in $Co_{0.5}Fe_{1.5}GeMo_3N$. The typical 1.6 T difference between the two internal hyperfine fields observed at 10 K results from a difference in the dipolar contribution to the hyperfine field at the iron-57 nuclide on the different sites.

The weighted average hyperfine field of 14.3 T found herein for Fe_2GeMo_3N and the 14.4 T observed[12] for $Co_{0.5}Fe_{1.5}GeMo_3N$ are very similar to the low-temperature hyperfine fields of 16.1, 10.9, and 9–15 T observed[25–27] for the face-centered iron site in MFe_3N, the perovskite-type nitrides, where M is Zn, Ru, or Ga. Similarly, low temperature magnetic moments of *ca.* 2 μ_B were observed[25,26] for the face-centered iron site in some of these perovskites. Hence, the complex nitrides studied herein and in ref. 12 have striking similarities with the perovskite-type nitrides in their magnetic and hyperfine characteristics.

There has been rather extensive theoretical work[25,26,28–30] on the relationship between the effective hyperfine field and the iron magnetic moment in the perovskite-type nitrides. One learns from this work that there are two main contributions to the hyperfine field, H_c^{core}, the negative core contribution arising from the 1s, 2s, and 3s electrons, and H_c^{val}, the positive valence contribution arising from the 3d and 4s electrons. The sum of these two contributions makes up the Fermi contact term, H_c. In the following discussion, the remaining contributions, *i.e.*, the dipolar and orbital contributions, contributions that are usually estimated[31,32] to be of the order of 10 percent of the effective field, will be ignored. The H_c^{core} and H_c^{val} contributions to the effective field are typically calculated to be *ca.* −24 and +10 T, respectively, to yield a net hyperfine field of −14 T. At this point one should note that, in the absence of an external applied magnetic field, only the magnitude of the hyperfine field may be obtained from Mössbauer spectral studies. $H_c^{core} = -24$ T is expected to be proportional to the iron magnetic moment of 2 μ_B, thus one obtains a proportionality constant of −12 T/μ_B. In Fe_2GeMo_3N, a magnetic moment of 1.90(4) μ_B is observed at 1.8 K and a H_c^{core} core contribution of −23 T is expected. If the observed hyperfine field is assumed to be negative and −14.3 T, a valence contribution, H_c^{val}, of +8.7 T results, a positive contribution that arises from the filling of the iron 3d band. This value is in reasonable agreement with that of +10 T observed for the iron perovskite-like nitrides.

Table 3 Calculated structural parameters for Fe_2GeMo_3N at 0 K^a

	Site	Bader partial charge	x	y	Z
Fe	32*e*	−0.3	0.2928	0.2928	0.2928
Ge	16*d*	−0.6	1/2	1/2	1/2
Mo	48*f*	+1.1	0.3181	1/8	1/8
N	16*c*	−2.1	0	0	0

[a] $a_0 = 11.1271$ Å.

(ii) Computational results

The lattice parameter and the fractional coordinates of the 32*e* and 48*f* sites calculated for Fe_2GeMo_3N, see Table 3, are in good agreement with experiment (*cf.* Table 1).

The calculated density of states for Fe_2GeMo_3N, see Fig. 6, is non-zero at the Fermi level, consistent with metallic conductivity. This is in agreement with the low experimental value for the resistivity reported above and the published experimental

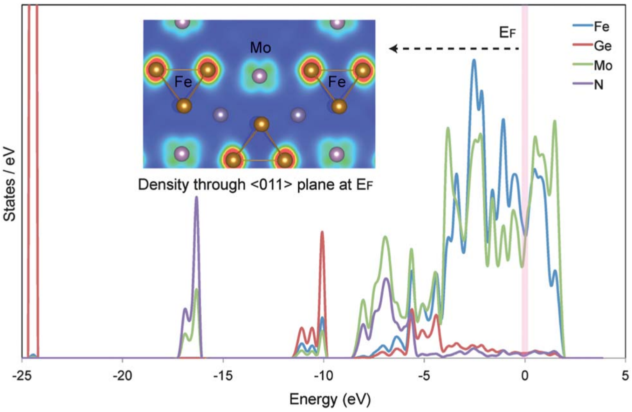

Fig. 6 The calculated density of states for antiferromagnetic Fe_2GeMo_3N at 0 K. The inset shows the charge density in the (011) plane at the Fermi energy.

Table 4 Calculated magnetic transition temperatures[a] for Fe_2GeMo_3N

No. of unpaired e^- on 32*e* site	$E_{AFM} - E_{FM}$/eV per unit cell	T^{MFA}/K	T^{RPA}/K	T^{MC1}/K	T^{MC2}/K
1.831	−1.3516	832	549	412	381

[a] Transition temperatures are calculated using the Heisenberg Hamiltonian with the QM mean-field approximation (T^{MFA}), the random-phase approximation (T^{RPA}) and classical Monte Carlo simulations on models 1 (T^{MC1}) and 2 (T^{MC2}).

data for Co_2GeMo_3N and Ni_2GeMo_3N.[12,33] The results of the Bader charge-density analysis, see Table 3, suggest that nitrogen atoms are reduced to diamagnetic anions with a complete octet of electrons. This is consistent with the assumption that nitrogen nominally exists as nitride (N^{3-}) ions in the η-carbide structure, the reduction in charge from −3e being a consequence of charge polarisation and a covalent component in the bonding. The charge on molybdenum is close to +1 while both transition metals and germanium have only small negative charges.

The calculated AFM-FM transition energy for Fe_2GeMo_3N is given in Table 4 along with the critical temperatures predicted at different levels of theory and the calculated number of unpaired electrons per atom. The calculated magnetic susceptibility of Fe_2GeMo_3N is shown in Fig. 2. In order to facilitate comparison with experiment, we have scaled the susceptibility maxima at the critical temperatures to be equal to the corresponding experimental value. Our calculations confirm the AFM nature of the coupling in this material; the calculated spin distribution in the ordered phase is consistent with the experimental data. On the whole, the agreement of the classical MC simulations with experiment is better than that of the QM analytical approximations. Curiously, but perhaps not surprisingly, making a classical approximation for S^2 in the RPA approaches leads to a critical temperature of 431 K, quite close to the result of the classical MC simulations and within just 25 K of the experimental value. Finally, no hysteresis was found in the data collected for Fe_2GeMo_3N during an additional longer run in which, after obtaining the last low-temperature spin configuration, we reversed the temperature changes so as to gradually reheat the system of spins.

5. Discussion

The experimental component of this study demonstrates that Fe_2GeMo_3N adopts the η-carbide structure with iron and germanium ordered over the 32*e* and 16*d* sites, respectively. The absence of hysteresis in the magnetic susceptibility immediately below the maximum observed at 455 K suggests that a transition from a paramagnetic to an antiferromagnetic phase occurs at this temperature. Neutron diffraction experiments carried out at temperatures of 300 K and below have confirmed the presence of antiferromagnetic ordering and suggested that the spin arrangement in the ordered phase is the same as that observed previously in compositions in the series $Fe_{2-x}Co_xGe_{1-y}Ga_yMo_3N$, although the ordered magnetic moment per 32*e* site is higher in the present case,[12] suggesting that the localized moment increases with increasing iron content. As a consequence of the disordered arrangement of Fe and Co over the 32*e* sites, the Mössbauer spectrum of $Fe_{1.5}Co_{0.5}GeMo_3N$ was very different to that recorded from Fe_2GeMo_3N and described above. The absence of atomic disorder in the present case has allowed us to use the spectra to show for the first time that the ordered spins align along a <111> direction in the antiferromagnetic phase; this information cannot be deduced from neutron diffraction data collected on a powder sample. Thus we have determined the antiferromagnetic spin-ordering pattern by neutron diffraction and the direction in which the spins align by Mössbauer spectroscopy. We note that the selection of just one of the equivalent <111> directions as the spin axis lowers the crystal symmetry to rhombohedral, but there was no evidence in the diffraction data for a loss of metric symmetry in the unit-cell parameters.

The sample dependence of the susceptibility below ~100 K, together with the absence of any marked change in the neutron diffraction pattern at 56 K, leads us to conclude that the transition apparent at the latter temperature in Fig. 2 is associated with the low-concentration impurity phase detected in the diffraction patterns, and not with Fe_2GeMo_3N.

The data described above demonstrate the sensitivity of the electronic properties of these interstitial nitrides to chemical composition. The reduction of the total electron count by one electron per transition-metal atom, such as occurs on passing from Co_2GeMo_3N to Fe_2GeMo_3N, results in a change from a compound that does not show long-range magnetic order to a compound with a Néel temperature as high as 455 K. Alternatively, the emphasis can be focussed on the 16*d* site, where the replacement of iron, from the d-block, by germanium, from the p-block, converts Fe_3Mo_3N, a complex, non-Fermi liquid, into Fe_2GeMo_3N, an antiferromagnet. A metallic conductivity is retained in all cases. This description emphasises the importance of both the 16*d* and 32*e* sites in determining the electronic properties of these materials. It also emphasises the importance of both the electron density and the energy of the valence orbitals of the constituent elements; comparison of the band structure of Fe_3Mo_3N (ref. 11) and that of Fe_2GeMo_3N shows that the valence orbitals of the atom on the 16*d* site make a much larger contribution to the density of states at the Fermi energy in the former than they do in the latter.

The calculations performed on Fe_2GeMo_3N had a number of successes. Most strikingly, the number of unpaired electrons (1.831) calculated to be at the 32*e* site is in excellent agreement with the ordered magnetic moment (1.90(4) μ_B) determined by neutron diffraction. However, calculations of the magnetic ordering temperature using either the MFA or the RPA within DFT resulted in overestimates. The transition temperatures calculated by MC methods were closer to the experimental value, erring on the low side. On a more positive note, whatever antiferromagnetic starting model was used in the calculations, the lowest-energy configuration corresponded to the experimentally observed structure.

6. Conclusions

In contrast to Fe_3Mo_3N and Co_3Mo_3N, Fe_2GeMo_3N provides an example of long-range magnetic ordering in the η-carbide structure; it is a metallic antiferromagnet below 455 K. A combination of neutron diffraction and Mössbauer spectroscopy was needed to determine the details of the magnetic structure, which consists of an antiferromagnetic arrangement of ferromagnetic Fe_4 tetrahedra. The number of unpaired electrons at the transition-metal site and the magnetic structure were successfully modelled by a combination of standard DFT and MC calculations, suggesting that complex compounds now lie within the scope of these techniques and that it should be possible to use them to predict the compositions that could become the magnetic materials of the future.

Acknowledgements

We are grateful to Thomas Hansen for experimental support at ILL, Grenoble and to S. Boyer for elemental analysis at London Metropolitan University. We acknowledge the use of the free classical MC code from Dr M. De Vries and HPC resources on HECToR, made available to us through the EPSRC-funded (EP/F067496) Materials Chemistry Consortium. F.G. acknowledges the financial support of the Fonds National de la Recherche Scientifique, grants 9.456595 and 1.5.064.05.

References

1 A. Westgren and G. Phragmen, *Trans. Am. Soc. Steel Treat.*, 1928, **13**, 539.
2 D. Errandonea, C. Ferrer-Roca, D. Martinez-Garcia, A. Segura, O. Gomis, A. Munoz, P. Rodriguez-Hernandez, J. Lopez-Solano, S. Alconchel and F. Sapina, *Phys. Rev. B: Condens. Matter Mater. Phys.*, 2010, **82**, 174105.
3 Y. Chen, J. Shen and N. Chen, *Solid State Commun.*, 2009, **149**, 121.
4 C. J. H. Jacobsen, *Chem. Commun.*, 2000, 1057.
5 S. Korlann, B. Diaz and M. E. Bussell, *Chem. Mater.*, 2002, **14**, 4049.
6 J. S. J. Hargreaves and D. Mckay, *J. Mol. Catal. A: Chem.*, 2009, **305**, 125.
7 D. Mckay, D. H. Gregory, J. S. J. Hargreaves, S. M. Hunter and X. Sun, *Chem. Commun.*, 2007, 3051.
8 S. M. Hunter, D. Mckay, R. I. Smith, J. S. J. Hargreaves and D. H. Gregory, *Chem. Mater.*, 2010, **22**, 2898.
9 S. Alconchel, F. Sapina, D. Beltran and A. Beltran, *J. Mater. Chem.*, 1998, **8**, 1901.
10 T. Waki, Y. Umemoto, S. Terazawa, Y. Tabata, A. Kondo, K. Sato, K. Kindo, S. Alconchel, F. Sapina, Y. Takahashi and H. Nakamura, *J. Phys. Soc. Jpn.*, 2010, **79**, 093703.
11 T. Waki, S. Terazawa, Y. Tabata, F. Oba, C. Michioka, K. Yoshimura, S. Ikeda, H. Kobayashi, K. Ohoyama and H. Nakamura, *J. Phys. Soc. Jpn.*, 2010, **79**, 043701.
12 L. A. Sviridov, P. D. Battle, F. Grandjean, G. J. Long and T. J. Prior, *Inorg. Chem.*, 2010, **49**, 1133.
13 T. Waki, S. Terazawa, T. Yamazaki, Y. Tabata, K. Sato, A. Kondo, K. Kindo, M. Yokoyama, Y. Takahashi and H. Nakamura, *Europhys. Lett.*, 2011, **94**, 37004.
14 R. N. Panda and N. S. Gajbhiye, *J. Alloys Compd.*, 1997, **256**, 102.
15 T. J. Prior and P. D. Battle, *J. Mater. Chem.*, 2004, **14**, 3001.
16 H. M. Rietveld, *J. Appl. Crystallogr.*, 1969, **2**, 65.
17 A. C. Larson and R. B. von Dreele, *General Structure Analysis System (GSAS), LAUR 86-748*, Los Alamos National Laboratories, 1994.
18 G. Kresse and J. Furthmuller, *Phys. Rev. B: Condens. Matter Mater. Phys.*, 1996, **54**, 11169.
19 J. Haffner, *J. Comput. Chem.*, 2008, **29**, 2044.
20 J. P. Perdew, A. Ruzsinszky, G. I. Csonka, O. A. Vydrov, G. E. Scuseria, L. A. Constantin, X. Zhou and K. Burke, *Phys. Rev. Lett.*, 2008, **100**, 136406.
21 P. E. Blochl, *Phys. Rev. B: Condens. Matter Mater. Phys.*, 1994, **50**, 17953.
22 A. Henkelman, A. Arnaldsson and H. Jonsson, *Comput. Mater. Sci.*, 2006, **36**, 354.
23 R. F. W. Bader, *Acc. Chem. Res.*, 1985, **18**, 9.
24 M. A. D. Vries, *Spinner, a Classical Monte Carlo Spin-lattice Simulation Program*, 2007, www.ccp5.ac.uk.
25 C. A. Kuhnen, R. S. D. Figueiredo and A. V. D. Santos, *J. Magn. Magn. Mater.*, 2000, **219**, 58.
26 C. Paduani, *J. Magn. Magn. Mater.*, 2004, **278**, 231.
27 J. Burghaus, M. Sougrati, A. Mochel, A. Houben, R. Hermann and R. Dronskowski, *J. Solid State Chem.*, 2011, **184**, 2315–2321.
28 X. G. Diao, R. B. Scorzelli and H. R. Rechenberg, *J. Magn. Magn. Mater.*, 2000, **218**, 81.
29 R. S. D. Figueredo, J. Foct, A. V. D. Santos and C. A. Kuhnen, *J. Alloys Compd.*, 2001, **315**, 42.
30 A. V. D. Santos and C. A. Kuhnen, *J. Alloys Compd.*, 2001, **321**, 60.
31 R. E. Watson and A. J. Freeman, in *Hyperfine Interactions*, ed. A. J. Freeman and R. B. Frankel, Academic Press, New York, 1967, p. 53.
32 R. E. Watson, in *Hyperfine Interactions*, eds. A. J. Freeman and R. B. Frankel, Academic Press, New York, 1967, p. 413.
33 L. A. Sviridov, D. Phil thesis, University of Oxford, 2009.